Tight power balance multi-time scale disposal strategy for wind integrated system considering electric vehicle charging station

Shengchun Yang[1], Yifan Chang[2] and Jun Xie[2]*

[1]China Electric Power Research Institute, Nanjing, China, [2]College of Energy and Electrical Engineering, Hohai University, Nanjing, China

High wind power penetration and peak load pose significant challenges to the power system in maintaining the power supply−demand balance. Once the power supply−demand balance is disrupted, system load shedding and wind spillage become inevitable. In this study, the aforementioned problem is defined as the tight power balance (TPB) problem. The accuracy of wind power and load forecasting increases with a decrease in the forecasting timescale. Based on the aforementioned characteristics, a TPB multi-timescale disposal strategy for wind-integrated power systems considering electric vehicle (EV) charging stations is established to address the TPB problem at different timescales. First, the operation model of an electric vehicle charging station offering flexible ramping capacity is established. Second, a multi-timescale disposal strategy, which includes an intra-day 4-h plan, an intra-day 1-h plan, and a real-time 15-min plan, is presented by quantifying the flexible demand at different timescales. Finally, the proposed strategy is verified using a modified IEEE 118-bus system. The analysis results show that the proposed TPB multi-timescale disposal strategy effectively promotes the disposal level of the TPB problem.

KEYWORDS

tight power balance disposal strategy, wind-integrated power system, electric vehicle charging station, multi-timescale, flexible ramping capacity, load shedding, wind spillage

1 Introduction

In response to the growing energy crisis and environmental pollution problems, increasing the share of renewable energy resources has become a roadmap for many nations (Ding et al., 2022; Han et al., 2022). However, with the large-scale integration of wind energy resources, the variability and uncertainty of the wind power output seriously affect the secure operation of the system (Khoshjahan et al., 2019; Park et al., 2022). The grid has to acquire adequate flexibility to satisfy the stochastic nature of the net load (the output of wind energy resources subtracted from the load) (Ghaljehei and Khorsand, 2022). Therefore, the exploration of system flexibility is of great significance for maintaining the secure operation of the power system.

Currently, many scholars have studied offering flexibility to power systems via flexible resources as a way of enhancing system flexibility. For example, electric vehicle (EV) charging stations (Zhang and Kezunovic, 2016), energy storage (Wang and Hodge, 2017; Khoshjahan et al., 2020), and flexible loads (Li et al., 2022) can offer flexibility to the power system, which reduces the regulation burden on thermal units. Heydarian-Forushani et al. (2018) devised an integrated stochastic day-ahead dispatching model, which included EV parking lots, bulk

energy storage, and demand response, to participate in the flexible ramp market. EV charging stations aggregate EVs to provide flexibility, fast response characteristics, and high social and economic benefits (Neyestani et al., 2015). To explore the possibility of EVs providing flexible ramping products, a novel distribution system locational marginal pricing (LMP) model has been presented (Zhang et al., 2020). Wu et al. (2015) modeled the operational flexibility of the day-ahead market, which included flexible resources such as demand–response and energy storage, for managing the variability of renewable energy sources. Nikoobakht et al. (2019) proposed a methodology to estimate the flexibility of a given day-ahead scheduling model. Zhang et al. (2016) developed an integrated day-ahead stochastic scheduling model to dispatch resources and deploy flexible ramping, with demand–response providing the required flexibility. Chang et al. (2022) proposed a disposal strategy for TPB considering electric vehicle charging stations that provide flexible ramping capacity. To cover the uncertainty of wind power, an information-gap decision theory (IGDT)–based robust security-constrained unit commitment (SCUC) model with the integration of demand–response (DR) was constructed (Mirzaei et al., 2019). However, the abovementioned studies have focused on enhancing system flexibility on a single timescale. To improve the accuracy of the scheduling results, the study of system flexibility on a multi-timescale has to be undertaken.

Related methods have been proposed for the study of system flexibility on a multi-timescale. To increase the economic efficiency of power system operations, Cui et al. (2017) developed a multi-timescale unit commitment model that considers flexible ramping requirements. A hybrid stochastic/deterministic multi-timescale scheduling model has been proposed to enhance flexible ramping (Shaaban et al., 2018). Yamujala et al. (2022) studied a two-stage flexibility-constrained scheduling issue with a day-ahead security-constrained unit commitment (DA-SCUC) and real-time security-constrained economic re-dispatch (RT-SCED) models, which accurately estimated and economically scheduled flexible ramp products. Olsen et al. (2020) conducted a Fourier analysis to disentangle the energy storage and power flexibility requirements on hourly and minute timescales. Mueller et al. (2019) efficiently exploited the flexibility of energy resources by considering multiple resources with complementary physical characteristics at different timescales. Bagherinezhad et al. (2020) proposed a look-ahead optimization model simulating day-ahead and real-time operations of power systems with flexible ramp products. A multi-timescale unit commitment and economic dispatch model considering solar power ramping products was developed to accurately estimate ramping requirements on a multi-timescale (Cui and Zhang, 2018).

With the widespread integration of wind energy resources into the existing power system, the power system operation is likely to face the following scenario. When facing a short-term peak load (Baniasadi et al., 2019), the installed capacity of the system generation is insufficient to supply the load. When the wind power is generated at its maximum with a relatively low system load, the system regulation capability is insufficient to completely accommodate the wind power. In such cases, the power supply and demand are unbalanced, which is defined as the TPB problem. The abovementioned studies investigated system flexibility without considering the impact of the TPB state on system flexibility. The TPB state further reduces the capability of the system to offer
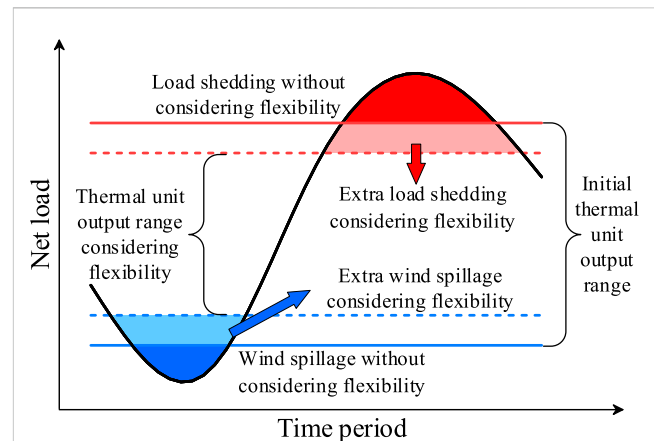

FIGURE 1
Schematic of the demand for flexibility limiting the thermal units' output range.

flexibility, resulting in extra load shedding and wind spillage. Moreover, the accuracy of wind power and load forecasting tends to increase with a decrease in the forecasting timescale (Hu et al., 2022). Therefore, a TPB multi-timescale disposal strategy should be developed to mitigate the effects of wind power and load forecasting errors on the power system.

The main contributions of this article are summarized as follows:

1) To address the TPB problem at different timescales, a TPB multi-timescale disposal framework is presented, and a TPB multi-timescale disposal strategy considering an EV charging station that offers flexible ramping capacity is developed to promote the disposal level of the TPB problem.
2) Based on the fact that the accuracy of wind power and load forecasting increases with a decrease in the forecasting timescale, the demand for flexibility is quantified at different timescales. Consequently, the effects of wind power and load forecasting errors on TPB disposal are mitigated, thereby reducing system load shedding and wind spillage.

The remainder of this article is organized as follows. Section 2 introduces the TPB multi-timescale disposal framework. Section 3 establishes the EV charging station operation model. Section 4 proposes a TPB multi-timescale disposal strategy. Section 5 analyzes and discusses a numerical example. Section 6 presents the conclusions of this article.

2 Tight power balance multi-timescale disposal framework

2.1 Demand for flexibility

In the TPB state, the capacity and regulation capability of the power system generation are insufficient to completely supply the load and accommodate wind power. High wind power penetration and peak load result in a high demand for flexibility. The system
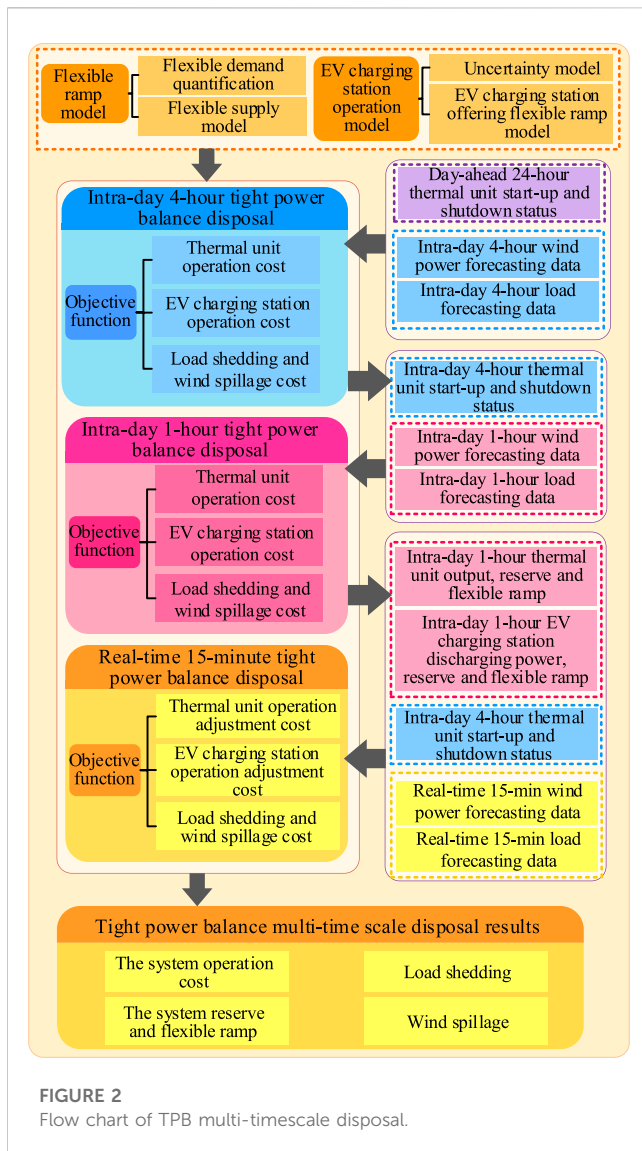
FIGURE 2
Flow chart of TPB multi-timescale disposal.

anti-peak load characteristics, which further cause load shedding and wind spillage.

2.2 Tight power balance multi-timescale disposal structure

Herein, the study of TPB multi-timescale disposal is divided into three timescales: an intra-day 4-h plan, an intra-day 1-h plan, and a real-time 15-min plan, with a time resolution of 15 min. Based on the fact that the accuracy of wind power and load forecasting increases with the decrease in forecasting timescale, a multi-timescale disposal strategy is developed to promote the disposal level of the TPB. The structure of TPB multi-timescale disposal is illustrated in Figure 2, and the detailed disposal structure is as follows:

1) Intra-day 4-h TPB disposal strategy. The TPB disposal strategy is formulated once every 4 h, with a time resolution of 15 min. Based on the intra-day 4-h wind power and load forecasting data, the thermal unit start-up and shutdown statuses and power output, charging and discharging statuses, and power of the EV charging station, system reserve, and flexible ramp are all updated over the next 4 h.

2) Intra-day 1-h TPB disposal strategy. The TPB disposal strategy is formulated once every 1 h, with a time resolution of 15 min. Based on the intra-day 4-h updated thermal unit start-up and shutdown statuses and the intra-day 1-h wind power and load forecasting data, the thermal unit power output, charging and discharging statuses, and power of the EV charging station, system reserve, and flexible ramp are all updated over the next 1 h.

3) Real-time 15-min TPB disposal strategy. The TPB disposal strategy is formulated once every 15 min, with a time resolution of 15 min. Based on the intra-day 4-h updated thermal unit start-up and shutdown statuses, the intra-day 1-h disposal results (thermal unit output, EV charging station discharging power, reserve, and flexible ramp offered by the thermal unit and EV charging station), and the real-time 15-min wind power and load forecasting data, the thermal unit output, charging and discharging statuses, and power of the EV charging station, system reserve, and flexible ramp are updated over the next 15 min.

3 Electric vehicle charging station operation model

EV charging stations are aggregators representing EVs involved in power, reserve, and flexible ramp scheduling (Heydarian-Forushani et al., 2018). In this section, the EV charging station uncertainty is first modeled. Subsequently, an EV charging station offering flexible ramping capacity is developed.

3.1 Electric vehicle charging station uncertainty model

EV charging station uncertainty is derived from the uncertain behavior of EVs, which include the number of EV arrivals and

demand for flexibility only offered by thermal units limits the output range of thermal units. As a result, the capability of the system to maintain the power supply–demand balance is weakened, resulting in load shedding and wind spillage.

As shown in Figure 1, in the TPB state, the capacity and regulation capability of the thermal units are both insufficient. When facing a peak load, load shedding is required, as illustrated in the dark red section of Figure 1. When facing high penetration of wind power, wind spillage is required, as illustrated in the dark blue section of Figure 1. The system flexibility offered by the thermal units limits their output range. The section between the dashed red and blue lines indicates the output range of the thermal units after they offer flexibility. During the peak load period, the requirement for thermal units to offer up-ramping lowers their maximum output, resulting in load shedding, as illustrated in the light red section of Figure 1. During the high wind power penetration period, the requirement for thermal units to offer down-ramping increases their minimum output, resulting in wind spillage, as illustrated in the light blue section of Figure 1. Additionally, wind power may have

departures, the initial state of energy (SOE) of EVs, and the capacity of EVs. Thus, to model EV charging station uncertainty, three groups of stochastic numbers based on the truncated normal distribution (Bessa, et al., 2012; Su and Chow, 2012) are employed, which are the arrival and departure times of EVs—t_n^{av}, t_n^{dp}; the initial state of charge (SOC) of EVs; and $soc_{cs,n,t_n^{arv},t^{dep}}^{EV}$. In addition, based on the probability distribution model of the capacity of EVs (Shafie-Khah, et al., 2016), 24 different types of capacities of EVs, $cap_{cs,n,t_n^{av},t_n^{dp}}^{EV}$, are employed.

3.1.1 Number of EVs in EV charging stations

The number of EVs that arrived at the EV charging station, cs, at t_n^{av} and departed from the EV charging station, cs, at t_n^{dp} can be formulated by the arrival and departure times of EVs in Eq. 1. The number of EVs in the EV charging stations, which is an uncertain parameter, is modeled in Eqs 2, 4.

$$N_{cs,t_n^{av},t_n^{dp}}^{EV} = \sum_n EV_{cs,n,t_n^{av},t_n^{dp}} \, t_n^{av} \in T_n^{av}, t_n^{dp} \in T_n^{dp}, \quad (1)$$

$$N_{cs,t}^{av} = \sum_{t_n^{dp}} N_{cs,t_n^{av},t_n^{dp}}^{EV}, \quad (2)$$

$$N_{cs,t}^{dp} = \sum_{t_n^{av}} N_{cs,t_n^{av},t_n^{dp}}^{EV}, \quad (3)$$

$$N_{cs,t}^{CS} = N_{cs,t-1}^{CS} + N_{cs,t}^{av} - N_{cs,t}^{dp}, \quad (4)$$

where $N_{cs,t_n^{av},t_n^{dp}}^{EV}$ is the number of EVs that arrived at the EV charging station, cs, at t_n^{av} and departed from the EV charging station, cs, at t_n^{dp}; $EV_{cs,n,t_n^{av},t_n^{dp}}$ is the EV_n that arrived at EV charging stations at t_n^{av} and departed from EV charging stations at t_n^{dp}; T_n^{av} and T_n^{dp} are the total number of periods of EV arrivals and departures; $N_{cs,t}^{av}$ is the total number of EVs that arrived at EV charging stations; $N_{cs,t}^{dp}$ is the total number of EVs that departed from EV charging stations; and $N_{cs,t}^{CS}$ is the total number of EVs in EV charging stations at t.

3.1.2 Initial SOE of EV charging stations

The SOE is the remaining energy of the EV capacity. The initial SOE of EV charging stations is obtained by aggregating the initial SOE of EV arrivals and departures, which is shown in Eqs 5–7.

$$E_{cs,t}^{av} = \sum_n \sum_{t_n^{dp}} soc_{cs,n,t_n^{av},t_n^{dp}}^{EV} cap_{cs,n,t_n^{av},t_n^{dp}}^{EV}, \quad (5)$$

$$E_{cs,t}^{dp} = \sum_n \sum_{t_n^{av}} soc_{cs,n,t_n^{av},t_n^{dp}}^{EV} cap_{cs,n,t_n^{av},t_n^{dp}}^{EV}, \quad (6)$$

$$E_{cs,t}^{CS,AD} = E_{cs,t-1}^{CS,AD} + E_{cs,t}^{av} - E_{cs,t}^{dp}, \quad (7)$$

where $E_{cs,t}^{av}$ is the initial SOE of EVs that arrived at EV charging stations; $soc_{cs,n,t_n^{av},t_n^{dp}}^{EV}$ is the initial SOC of EV arrivals and departures; $cap_{cs,n,t_n^{av},t_n^{dp}}^{EV}$ is the capacity of EV arrivals and departures; $E_{cs,t}^{dp}$ is the initial SOE of EVs that departed from EV charging stations; and $E_{cs,t}^{CS,AD}$ is the total initial SOE of EV charging stations at t.

3.1.3 Total capacity of EV charging stations

The total capacity of EV charging stations is obtained by aggregating the capacity of EV arrivals and departures, which is shown in Eqs 8–10.

$$CAP_{cs,t}^{av} = \sum_n \sum_{t_n^{dp}} cap_{cs,n,t_n^{av},t_n^{dp}}^{EV}, \quad (8)$$

$$CAP_{cs,t}^{dp} = \sum_n \sum_{t_n^{av}} cap_{cs,n,t_n^{av},t_n^{dp}}^{EV}, \quad (9)$$

$$CAP_{cs,t}^{CS,AD} = CAP_{cs,t-1}^{CS,AD} + CAP_{cs,t}^{av} - CAP_{cs,t}^{dp}, \quad (10)$$

where $CAP_{cs,t}^{av}$ is the capacity of EVs that arrived at EV charging stations, $CAP_{cs,t}^{dp}$ is the capacity of EVs that departed from EV charging stations, and $CAP_{cs,t}^{CS,AD}$ is the total capacity of EV charging stations at t.

3.2 Model for electric vehicle charging station offering flexible ramping capacity

The EV charging stations can offer up-ramping in the vehicle-to-grid (V2G) mode and down-ramping in the grid-to-vehicle (G2V) mode. The EV charging stations that offer flexible ramping capacity are limited by the charging and discharging rate, capacity, and SOE of the EV charging stations.

3.2.1 Charging and discharging rate constraints of EV charging station

The power, reserve, and flexible ramp of EV charging stations are constrained by their charging and discharging rates, as shown in Eqs 11–13.

$$\begin{aligned} p_{cs,t}^{CS,CS2G} + FR_{cs,t}^{CS,up} + SR_{cs,t}^{CS} + NSR_{cs,t}^{CS} + RGR_{cs,t}^{CS,up} \\ + RPR_{cs,t}^{CS} \leq \eta^{dis} N_{cs,t}^{CS} u_{cs,t}^{CS2G}, \end{aligned} \quad (11)$$

$$p_{cs,t}^{CS,G2PL} + FR_{cs,t}^{CS,dn} + RGR_{cs,t}^{CS,dn} \leq \eta^{ch} N_{cs,t}^{CS} u_{cs,t}^{G2CS}, \quad (12)$$

$$u_{cs,t}^{CS2G} + u_{cs,t}^{G2CS} \leq 1, \quad (13)$$

where $p_{cs,t}^{CS,CS2G}$ and $p_{cs,t}^{CS,G2PL}$ are the power from EV charging stations to the grid and from the grid to EV charging stations, respectively; $FR_{cs,t}^{CS,up}$ and $FR_{cs,t}^{CS,dn}$ are the up-ramping and down-ramping offered by EV charging stations, respectively; $SR_{cs,t}^{CS}$ and $NSR_{cs,t}^{CS}$ are the spinning and non-spinning reserves offered by EV charging stations, respectively; $RGR_{cs,t}^{CS,up}$ and $RGR_{cs,t}^{CS,dn}$ are the upregulation and downregulation reserves offered by EV charging stations, respectively; $RPR_{cs,t}^{CS}$ is the replacement reserve offered by EV charging stations; η^{dis} and η^{ch} are the discharging and charging rates of EVs; $u_{cs,t}^{CS2G}$ and $u_{cs,t}^{G2CS}$ are the states of power from EV charging stations to the grid and from the grid to EV charging stations, respectively.

3.2.2 SOE coupling constraints of EV charging stations in adjacent periods

The SOE of EV charging stations in a period is affected by the SOE of EV charging stations in the previous period, EVs arrival and departure, charging and discharging power, offered reserve, and flexible ramp, as shown in Eq. 14

$$\begin{aligned} E_{cs,t}^{CS} = E_{cs,t-1}^{CS} + E_{cs,t}^{av} - E_{cs,t}^{dp} \\ + \xi_{ch}^{CS} \left(p_{cs,t}^{CS,G2CS} + FR_{cs,t}^{CS,dn} + RGR_{cs,t}^{CS,dn} \right) \\ - {1}/{\xi_{dis}^{CS}} \left(p_{cs,t}^{CS,CS2G} + FR_{cs,t}^{CS,up} + SR_{cs,t}^{CS} \right. \\ + NSR_{cs,t}^{CS} + RGR_{cs,t}^{CS,up} + RPR_{cs,t}^{CS} \left. \right) \end{aligned} \quad (14)$$

where $E_{cs,t}^{CS}$ is the SOE of EV charging stations, and ξ_{ch}^{CS} and ξ_{dis}^{CS} are the charging and discharging efficiencies of the EV charging stations, respectively.
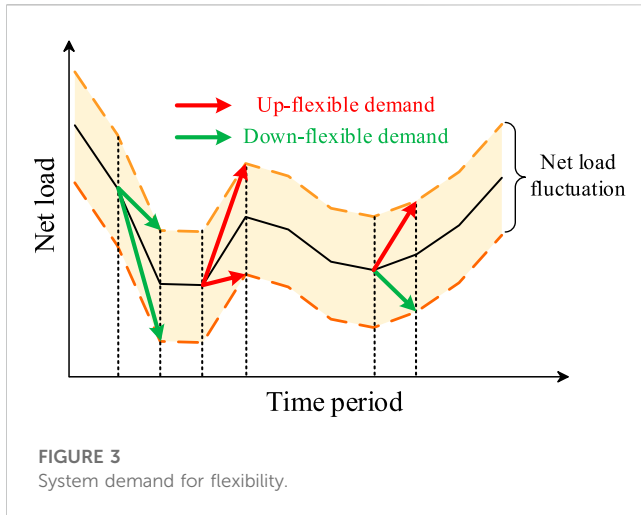
FIGURE 3
System demand for flexibility.

3.2.3 Power exchange limit with grid of EVs in V2G mode constraints

A contract is signed between EV charging stations and EVs to permit EV charging stations to utilize the V2G mode of EVs (Neyestani, et al., 2015; Shafie-Khah et al., 2016). EV charging stations aggregate the SOC demand allocated for each period to limit power exchange with the grid, as shown in Eq. 15

$$
\begin{aligned}
P_{cs,t}^{CS,CS2G} + FR_{cs,t}^{CS,up} + SR_{cs,t}^{CS} + NSR_{cs,t}^{CS} + RGR_{cs,t}^{CS,up} \\
+ RPR_{cs,t}^{CS} \leq \chi_{cs,t} E_{cs,t}^{CS,AD},
\end{aligned}
\tag{15}
$$

where $\chi_{cs,t}$ is the percentage of net discharge due to the SOC demand signed for EVs.

3.2.4 Upper and lower limits of SOC and SOE of EV charging station constraints

$$
soc_{cs,n}^{EV,min} \leq soc_{cs,n,t}^{EV} \leq soc_{cs,n}^{EV,max}, \tag{16}
$$

$$
\underbrace{\sum_{n} soc_{cs,n}^{EV,min}}_{SOC_{cs}^{CS,min}} \leq SOC_{cs,t}^{CS} \leq \underbrace{\sum_{n} soc_{cs,n}^{EV,max}}_{SOC_{cs}^{CS,max}}, \tag{17}
$$

$$
SOC_{cs}^{CS,min} CAP_{cs,t}^{CS,AD} \leq E_{cs,t}^{CS} \leq SOC_{cs}^{CS,max} CAP_{cs,t}^{CS,AD}, \tag{18}
$$

where $soc_{cs,n,t}^{EV}$ is the SOC of EVs; $soc_{cs,n}^{EV,max}$ and $soc_{cs,n}^{EV,min}$ are the upper and lower limits of the SOC of EVs, respectively; $SOC_{cs,t}^{CS}$ is the SOC of EV charging stations; and $SOC_{cs}^{CS,max}$ and $SOC_{cs}^{CS,min}$ are the upper and lower limits of the SOC of EV charging stations, respectively.

4 Tight power balance multi-timescale disposal strategy

4.1 System flexible demand

The demand for flexibility originates from the variability and uncertainty of the system net load. The value of the subtraction of the net load of the previous period from that of the next period is

obtained. A positive value indicates the demand for up-flexibility, while a negative value indicates the demand for down-flexibility, as shown in Figure 3.

The range of net load fluctuation is calculated from the forecasting errors of wind power and load, and thus the system demand for flexibility is acquired, as shown in Eqs 19–21.

$$
\varepsilon_t = \max\left(\left|\varepsilon_t^{WP}\right|, \left|\varepsilon_t^{LD}\right|\right), \tag{19}
$$

$$
\begin{cases}
NL_t^{max} = (1 + \varepsilon_t)NL_t \\
NL_t^{min} = (1 - \varepsilon_t)NL_t
\end{cases}, \tag{20}
$$

$$
\begin{cases}
FRN_t^{up} = \max\left(0, NL_t^{max} - NL_{t-1}\right) \\
FRN_t^{dn} = \max\left(0, NL_{t-1} - NL_t^{min}\right)
\end{cases}, \tag{21}
$$

where ε_t^{WP} and ε_t^{LD} are the forecasting errors of the wind power and load, respectively; ε_t is the net load fluctuation factor; NL_t is the system net load; NL_t^{max} and NL_t^{min} are the limitations of the net load fluctuation range; and FRN_t^{up} and FRN_t^{dn} are the system demands for up-flexibility and down-flexibility, respectively.

At different timescales, the system demand for flexibility varies with the forecasting accuracy of the wind and load. As the timescale continues to shorten, the forecasting accuracy of the wind power and load continues to improve, the forecasting error decreases, and the system demand for flexibility decreases.

4.2 Intra-day 4-h tight power balance disposal strategy

The intra-day 4-h TPB disposal strategy is formulated once every 4 h with a time resolution of 15 min. Based on the intra-day 4-h wind power and load forecasting data, the thermal unit start-up and shutdown statuses and power output, charging and discharging statuses, and power of the EV charging station, system reserve, and flexible ramp are all updated for the next 4 h.

4.2.1 Objective function

The objective function of the intra-day 4-h TPB disposal strategy is to minimize the total system operation cost, which includes the thermal unit operation cost, EV charging station operation cost, load shedding cost, and wind spillage cost, as shown in Eqs 22–27.

Eq. 22 is the total system operation cost; Eq. 23 is the thermal unit operation cost, which includes the thermal unit fuel cost, start-up cost, reserve, and flexible ramp cost; Eq. 24 is the thermal unit fuel cost; Eq. 25 is the EV charging station operation cost, which includes the EV charging station discharging cost, battery depreciation cost, reserve, and flexible ramp cost; Eq. 26 is the EV charging station battery depreciation cost, while Eq. 27 is the load shedding and wind spillage cost.

$$
\min C^{ID,4h} = C_{TU}^{ID,4h} + C_{CS}^{ID,4h} + C_{WL}^{ID,4h}, \tag{22}
$$

$$
\begin{aligned}
C_{TU}^{ID,4h} = \sum_{t=1}^{N_T}\sum_{tu=1}^{N_{TU}} \Big[& u_{tu,t}C_{tu,t}^F + S_{tu,t}u_{tu,t}\left(1 - u_{tu,t-1}\right) \\
& + \gamma_{tu,t}^{TU,sr}SR_{tu,t}^{TU} + \gamma_{tu,t}^{TU,nsr}NSR_{tu,t}^{TU} + \gamma_{tu,t}^{TU,rgr}RGR_{tu,t}^{TU,up} \\
& + \gamma_{tu,t}^{TU,rgr}RGR_{tu,t}^{TU,dn} + \gamma_{tu,t}^{TU,rpr}RPR_{tu,t}^{TU} \\
& + \gamma_{tu,t}^{TU,up}FR_{tu,t}^{TU,up} + \gamma_{tu,t}^{TU,dn}FR_{tu,t}^{TU,dn} \Big]
\end{aligned}
\tag{23}
$$

$$
C_{tu,t}^F = a_{tu}p_{tu,t}^2 + b_{tu}p_{tu,t} + c_{tu}, \tag{24}
$$

$$C_{CS}^{ID,4h} = \sum_{t=1}^{N_T} \sum_{cs=1}^{N_{CS}} \left[\gamma_{cs,t}^{CS,cs2g} p_{cs,t}^{CS,CS2G} + \gamma_{cs,t}^{CS,sr} SR_{cs,t}^{CS} \right.$$
$$+ \gamma_{cs,t}^{CS,nsr} NSR_{cs,t}^{CS} + \gamma_{cs,t}^{CS,rgr} RGR_{cs,t}^{CS,up}$$
$$+ \gamma_{cs,t}^{CS,rgr} RGR_{cs,t}^{CS,dn} + \gamma_{cs,t}^{CS,rpr} RPR_{cs,t}^{CS} \qquad (25)$$
$$\left. + \gamma_{cs,t}^{CS,up} FR_{cs,t}^{CS,up} + \gamma_{cs,t}^{CS,dn} FR_{cs,t}^{CS,dn} + C_{cs,t}^{BD} \right],$$

$$C_{cs,t}^{BD} = C^{BDC} \left(p_{cs,t}^{CS,CS2G} + p_{cs,t}^{CS,G2CS} \right) \sigma, \qquad (26)$$

$$C_{WL}^{ID,4h} = \sum_{t=1}^{N_T} \left[\sum_{w=1}^{N_{WP}} \gamma_{w,t}^{WP,spl} P_{w,t}^{WP,spl} + \sum_{b=1}^{N_B} \gamma_{b,t}^{LD,shed} LD_{b,t}^{shed} \right], \qquad (27)$$

where, in Eq. 22, $C^{ID,4h}$ is the intra-day 4-h total system operation cost, $C_{TU}^{ID,4h}$ is the thermal unit operation cost, $C_{CS}^{ID,4h}$ is the EV charging station operation cost, and $C_{WL}^{ID,4h}$ is the load shedding and wind spillage cost. In Eq. 23, N_T is the total number of intra-day 4-h TPB disposal periods; N_{TU} is the total number of thermal units; $u_{tu,t}$ is the start-up and shutdown statuses of the thermal units; $S_{tu,t}$ is the thermal unit start-up cost; $C_{tu,t}^F$ is the thermal unit fuel cost; $\gamma_{tu,t}^{TU,sr}$ and $\gamma_{tu,t}^{TU,nsr}$ are the thermal unit spinning and non-spinning reserve cost coefficient, respectively; $SR_{tu,t}^{TU}$ and $NSR_{tu,t}^{TU}$ are the spinning and non-spinning reserve offered by thermal units; $\gamma_{tu,t}^{TU,rgr}$ and $\gamma_{tu,t}^{TU,rpr}$ are the thermal unit regulation and replacement reserve cost coefficients, respectively; $RGR_{tu,t}^{TU,up}$ and $RGR_{tu,t}^{TU,dn}$ are the upregulation and downregulation reserve offered by thermal units; $RPR_{tu,t}^{TU}$ is the replacement reserve offered by thermal units; $\gamma_{tu,t}^{TU,up}$ and $\gamma_{tu,t}^{TU,dn}$ are the thermal unit up-flexible ramp and down-flexible ramp cost coefficients, respectively; and $FR_{tu,t}^{TU,up}$ and $FR_{tu,t}^{TU,dn}$ are the up-flexible ramp and down-flexible ramp offered by thermal units. In Eq. 24, $p_{tu,t}$ is the thermal unit output, and a_{tu}, b_{tu}, and c_{tu} are the thermal unit fuel cost coefficients. In Eq. 25, N_{CS} is the total number of EV charging stations; $\gamma_{cs,t}^{CS,cs2g}$ is the EV charging station discharging cost coefficient; $C_{cs,t}^{BD}$ is the EV charging station battery depreciation cost; $\gamma_{cs,t}^{CS,sr}$ and $\gamma_{cs,t}^{CS,nsr}$ are the EV charging station spinning and non-spinning reserve cost coefficients, respectively; $\gamma_{cs,t}^{CS,rgr}$ and $\gamma_{cs,t}^{CS,rpr}$ are the EV charging station regulation and replacement reserve cost coefficients, respectively; and $\gamma_{cs,t}^{CS,up}$ and $\gamma_{cs,t}^{CS,dn}$ are the EV charging station up-flexible ramp and down-flexible ramp cost coefficients, respectively. In Eq. 26, C^{BDC} is the battery charging and discharging loss coefficient, and σ is the TPB disposal time resolution. In Eq. 27, N_B and N_{WP} are the total number of loads and wind power units, respectively; $\gamma_{w,t}^{WP,spl}$ and $\gamma_{b,t}^{LD,shed}$ are the wind spillage and load shedding cost coefficients, respectively; and $P_{w,t}^{WP,spl}$ and $LD_{b,t}^{shed}$ are the wind spillage and load shedding, respectively.

4.2.2 Constraints

4.2.2.1 Thermal unit operational constraints

The thermal unit operation constraints include the thermal unit up-ramping and down-ramping capacity constraints, shown in Eqs 28, 29, and the thermal unit output maximum and minimum constraints, shown in Eqs 30, 31.

$$FR_{tu,t}^{TU,up} + SR_{tu,t}^{TU} + NSR_{tu,t}^{TU} + RGR_{tu,t}^{TU,up} + RPR_{tu,t}^{TU} \leq R_{tu}^{TU,up} \sigma, \qquad (28)$$

$$FR_{tu,t}^{TU,dn} + RGR_{tu,t}^{TU,dn} \leq R_{tu}^{TU,dn} \sigma, \qquad (29)$$

$$p_{tu,t} + FR_{tu,t}^{TU,up} + SR_{tu,t}^{TU} + NSR_{tu,t}^{TU} + RGR_{tu,t}^{TU,up} + RPR_{tu,t}^{TU} \leq u_{tu,t} p_{tu}^{max}, \qquad (30)$$

$$p_{tu,t} - FR_{tu,t}^{TU,dn} - RGR_{tu,t}^{TU,dn} \geq u_{tu,t} p_{tu}^{min}, \qquad (31)$$

where $R_{tu}^{TU,up}$ and $R_{tu}^{TU,dn}$ are the thermal unit's up- and down-ramping rates, respectively, and p_{tu}^{max} and p_{tu}^{min} are the thermal unit maximum and minimum outputs, respectively.

4.2.2.2 Operational constraints of EV charging stations

The electric vehicle charging station operation constraints have been listed in Eqs 1–18 and are, therefore, not presented here.

4.2.2.3 Wind power unit operational constraints

The wind power unit operation constraints include the wind power unit's maximum and minimum output and system wind spillage constraints, as shown in Eqs 32, 33, and the flexible ramping capacity offered by the wind power unit constraint is shown in Eq. 34:

$$0 \leq p_{w,t}^{WP} \leq p_{w,t}^{WP,max}, \qquad (32)$$

$$P_{w,t}^{WP,spl} = p_{w,t}^{WP,max} - p_{w,t}^{WP}, \qquad (33)$$

$$\begin{cases} FR_{w,t}^{WP,up} = \max\left(p_{w,t}^{WP} - p_{w,t-1}^{WP}, 0 \right) \\ FR_{w,t}^{WP,dn} = \max\left(p_{w,t-1}^{WP} - p_{w,t}^{WP}, 0 \right) \end{cases}, \qquad (34)$$

where $p_{w,t}^{WP}$ is the wind power output, $p_{w,t}^{WP,max}$ is the wind power maximum and minimum outputs, and $FR_{w,t}^{WP,up}$ and $FR_{w,t}^{WP,dn}$ are the up-flexible ramp and down-flexible ramp offered by the wind power units.

4.2.2.4 System demand for up-flexible and down-flexible constraints

The demand of the system for flexibility can be supplied by thermal units, EV charging stations, and wind power units. In extreme scenarios, the system demand for flexibility can be offered by load shedding and wind spillage, which will cause a significant rise in the operation cost, as shown in Eqs 35–37.

$$\begin{cases} FR_t^{LD,shed,up} = \sum_{b \in N_B} LD_{b,t}^{shed} \\ FR_t^{WP,spl,dn} = \sum_{w \in N_{WP}} P_{w,t}^{WP,spl} \end{cases}, \qquad (35)$$

$$\sum_{tu=1}^{N_{TU}} FR_{tu,t}^{TU,up} + \sum_{w=1}^{N_{WP}} FR_{w,t}^{WP,up} + \sum_{cs=1}^{N_{CS}} FR_{cs,t}^{CS,up} + FR_t^{LD,shed,up} \geq FRN_t^{up}, \qquad (36)$$

$$\sum_{tu=1}^{N_{TU}} FR_{tu,t}^{TU,dn} + \sum_{w=1}^{N_{WP}} FR_{w,t}^{WP,dn} + \sum_{cs=1}^{N_{CS}} FR_{cs,t}^{CS,dn} + FR_t^{WP,spl,dn} \geq FRN_t^{dn}, \qquad (37)$$

where $FR_t^{LD,shed,up}$ and $FR_t^{WP,spl,dn}$ are the up-flexible ramp offered by load shedding and the down-flexible ramp offered by wind spillage, respectively.

4.2.2.5 System power supply–demand balance constraint

$$\sum_{tu=1}^{N_{TU}} p_{tu,t} + \sum_{w=1}^{N_{WP}} p_{w,t}^{WP} + \sum_{cs=1}^{N_{CS}} \left(p_{cs,t}^{CS,CS2G} - p_{cs,t}^{CS,G2CS} \right) = \sum_{b=1}^{N_B} \left(LD_{b,t} - LD_{b,t}^{shed} \right), \qquad (38)$$

$$0 \leq LD_{b,t}^{shed} \leq \delta^{shed} LD_{b,t}, \qquad (39)$$

where $LD_{b,t}$ is the system load and δ^{shed} is the load shedding rate (the proportion of maximum load shedding to the system load).

TABLE 1 EV charging station parameters.

$\eta^{dis/ch}$/kW h^{-1}	$\xi_{dis/ch}^{CS}$/%	$\chi_{cs,t}$/%	$SOC_{cs}^{CS,\,max}$/%	$SOC_{cs}^{CS,\,min}$/%
22	90	40	90	30

TABLE 2 Intra-day 4-h and multi-timescale TPB disposal.

Case	Timescale	Integration of EV charging stations
Case 1	Intra-day 4-h	No
Case 2	Intra-day 4-h	Yes
Case 3	Multi-timescale	No
Case 4	Multi-timescale	Yes

4.3 Intra-day 1-h tight power balance disposal strategy

The intra-day 1-h TPB disposal strategy is formulated once every 1 h with a time resolution of 15 min. Based on the start-up and shutdown statuses of the intra-day 4-h updated thermal unit and intra-day 1-h wind power and load forecasting data, the thermal unit's output, charging and discharging statuses, and power of the EV charging station, system reserve, and flexible ramp are updated for the next 1 h.

4.3.1 Objective function

The objective function of the intra-day 1-h TPB disposal strategy is basically the same as that of the intra-day 4-h TPB disposal strategy, but the start-up cost of the thermal units is not considered. The objective function minimizes the total system operation cost, which includes the thermal unit operation cost, EV charging station operation cost, load shedding cost, and wind spillage cost.

$$\min C^{ID,1h} = C_{TU}^{ID,1h} + C_{CS}^{ID,1h} + C_{WL}^{ID,1h}. \quad (40)$$

4.3.2 Constraints

The constraints of the intra-day 1-h TPB disposal strategy are basically the same as those of the intra-day 4-h TPB disposal strategy, which include the thermal unit operation constraints (Eqs 28–31), EV charging station operation constraints (Eqs 1–18), wind power, system flexibility, and load constraints (Eqs 19–21, 32–39), which are not presented here.

4.4 Real-time 15-min tight power balance disposal strategy

The real-time 15-min TPB disposal strategy is formulated once every 15 min with a time resolution of 15 min. Based on the start-up and shutdown statuses of the intra-day 4-h updated thermal unit and the real-time 15-min wind power and load forecasting data, the thermal unit output, charging and discharging statuses of the EV

charging station, and power, system reserve, and flexible ramp are updated for the next 15 min.

4.4.1 Objective function

The objective function of the real-time 15-min TPB disposal strategy is to minimize the total operation adjustment cost between the real-time 15-min and intra-day 1-h TPB disposal, which include the thermal unit operation adjustment cost, EV charging station operation adjustment cost, load shedding cost, and wind spillage cost, as shown in Eqs 41–44.

Eq. 41 is the total operation adjustment cost of the system, and Eq. 42 is the thermal unit operation adjustment cost, which include the thermal unit output adjustment cost, reserve, and flexible ramp adjustment cost; Eq. 43 is the EV charging station operation adjustment cost, which include the EV charging station discharging adjustment cost, battery depreciation cost, reserve, and flexible ramp adjustment cost. Eq. 44 is the load shedding and wind spillage cost.

$$\min C^{RT,15\min} = C_{TU}^{RT,15\min} + C_{CS}^{RT,15\min} + C_{WL}^{RT,15\min}, \quad (41)$$

$$
\begin{aligned}
C_{TU}^{RT,15\min} = \sum_{t=1}^{N_T^{RT}} \sum_{i=1}^{N_{TU}} \Big[& \mu_{tu,t}^{TU} u_{tu,t} \left| \Delta p_{tu,t} \right| + \mu_{tu,t}^{TU,sr} \left| \Delta SR_{tu,t}^{TU} \right| \\
& + \mu_{tu,t}^{TU,nsr} \left| \Delta NSR_{tu,t}^{TU} \right| + \mu_{tu,t}^{TU,rgr} \left| \Delta RGR_{tu,t}^{TU,up} \right| \\
& + \mu_{tu,t}^{TU,rgr} \left| \Delta RGR_{tu,t}^{TU,dn} \right| + \mu_{tu,t}^{TU,rpr} \left| \Delta RPR_{tu,t}^{TU} \right| \\
& + \mu_{tu,t}^{TU,up} \left| \Delta FR_{tu,t}^{TU,up} \right| + \mu_{tu,t}^{TU,dn} \left| \Delta FR_{tu,t}^{TU,dn} \right| \Big],
\end{aligned}
\quad (42)
$$

$$
\begin{aligned}
C_{CS}^{RT,15\min} = \sum_{t=1}^{N_T^{RT}} \sum_{cs=1}^{N_{CS}} \Big[& \mu_{cs,t}^{CS,cs2g} \left| \Delta P_{cs,t}^{CS,CS2G} \right| + \mu_{cs,t}^{CS,sr} \left| \Delta SR_{cs,t}^{CS} \right| \\
& + \mu_{cs,t}^{CS,nsr} \left| \Delta NSR_{cs,t}^{CS} \right| + \mu_{cs,t}^{CS,rgr} \left| \Delta RGR_{cs,t}^{CS,up} \right| \\
& + \mu_{cs,t}^{CS,rgr} \left| \Delta RGR_{cs,t}^{CS,dn} \right| + \mu_{cs,t}^{CS,rpr} \left| \Delta RPR_{cs,t}^{CS} \right| \\
& + \mu_{cs,t}^{CS,up} \left| \Delta FR_{cs,t}^{CS,up} \right| + \mu_{cs,t}^{CS,dn} \left| \Delta FR_{cs,t}^{CS,dn} \right| + C_{cs,t}^{BD} \Big],
\end{aligned}
\quad (43)
$$

$$
C_{WL}^{RT,15\min} = \sum_{t=1}^{N_T^{RT}} \left[\sum_{w=1}^{N_{WP}} \gamma_{w,t}^{WP,spl} P_{w,t}^{WP,spl} + \sum_{b=1}^{N_B} \gamma_{b,t}^{LD,shed} LD_{b,t}^{shed} \right], \quad (44)
$$

where $C^{RT,15\min}$ is the real-time 15-min system total operation adjustment cost; $C_{TU}^{RT,15\min}$ is the real-time 15-min thermal unit operation adjustment cost; N_T^{RT} is the total number of real-time 15-min TPB disposal periods; $C_{CS}^{RT,15\min}$ is the real-time 15-min EV charging station operation adjustment cost; $C_{WL}^{RT,15\min}$ is the real-time 15-min load shedding and wind spillage cost; $\Delta(\cdot)$ is the adjustment of thermal unit output, reserve, and flexible ramp, with EV charging station discharging between the real-time 15-min and intra-day 1-h TPB disposal; $\mu_{tu,t}^{TU}$ is the thermal unit output adjustment cost coefficient; $\mu_{tu,t}^{TU,(\cdot)}$ is the thermal unit reserve and flexible ramp adjustment cost coefficient; and $\mu_{cs,t}^{CS,(\cdot)}$ is the EV charging station discharging, reserve, and flexible ramp cost coefficients.

4.4.2 Constraints

The constraints of the real-time 15-min TPB disposal strategy are basically the same as those of the intraday 4-h strategy, which include the thermal unit operation constraints (Eqs 28–31), the EV charging station operation constraints (Eqs 1–18), the wind power, system flexibility, and load constraints (Eqs 19–21, 32–39), which are not presented here.

TABLE 3 TPB multi-timescale disposal results.

| Case	Total operation cost/$	Load shedding/MWh	Wind spillage/MWh	Thermal unit flexible ramp/MWh	Thermal unit flexible ramp saving/MWh
Case 1	1,101,507.99	3,133.71	1,247.50	2,540.54	0
Case 2	875,856.58	1,880.57	450.78	2,246.44	1,759.62
Case 3	653,011.06	1,215.44	4.35	2,083.80	0
Case 4	548,199.35	641.66	0	1,141.53	1,356.11

5 Numerical example

In this study, numerical simulations were conducted on a modified IEEE 118-bus system (Cui, et al., 2017) to verify the effectiveness of the proposed TPB multi-timescale disposal strategy. The EV charging stations were aggregated into 10 charging stations, each comprising 13,500 charging spots, integrated into the grid. Wind power output, load forecasting data, and actual data were extracted from the study by Heydarian-Forushani et al. (2018). The thermal unit reserve, flexible ramp capacity, and cost were obtained from the study by Heydarian-Forushani et al. (2015). The load shedding and wind spillage costs were 200 \$ MWh^{-1} and 40 \$ MWh^{-1}, respectively (Heydarian-Forushani, et al., 2018). To simulate EV charging station uncertainty, the number of EVs in the EV charging stations, SOE, and capacity of the EV charging stations were acquired. The EV charging station parameters are presented in Table 1 (Heydarian-Forushani, et al., 2018). The proposed TPB multi-timescale disposal strategy for wind integrated power systems considering EV charging stations was implemented on MATLAB R2018a using the YALMIP toolbox and solved by the ILOG CPLEX 12.8 on a personal Dell computer with an Intel 2.6-GHz dual-core processor and 6 GB of RAM. For each TPB multi-timescale disposal strategy in the numerical simulations, the optimal solutions were found within 562 s.

5.1 Analysis of tight power balance multi-timescale disposal results

On a multi-timescale, to investigate the impact of the integration of EV charging stations on load shedding and wind spillage problems, four cases were set up to analyze the results, as presented in Table 2.

For different cases, the total system operation cost, load shedding, wind spillage, thermal unit flexible ramp, and thermal unit flexible ramp savings are listed in Table 3. The thermal unit flexible ramp saving indicates the flexible ramping capacity offered by the EV charging stations.
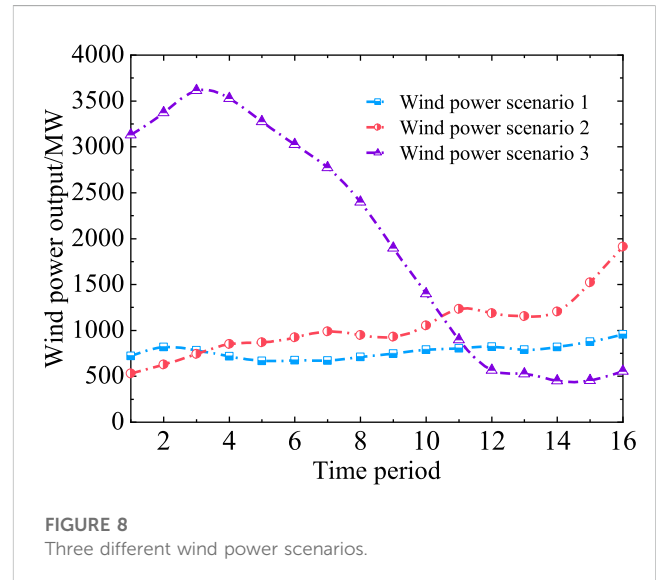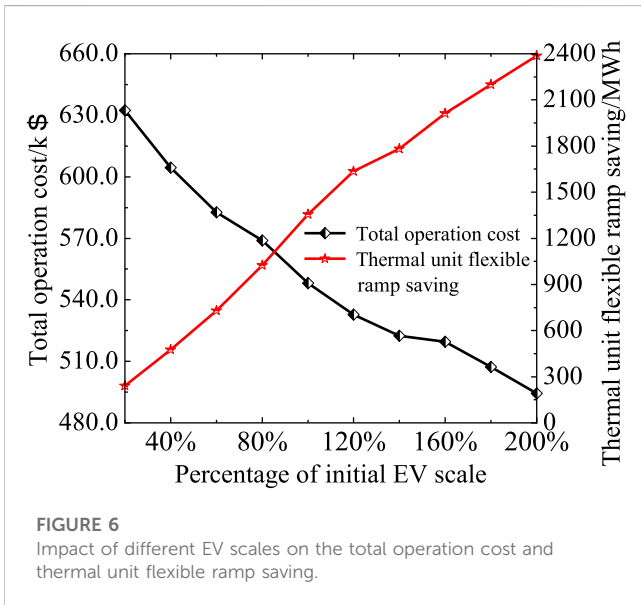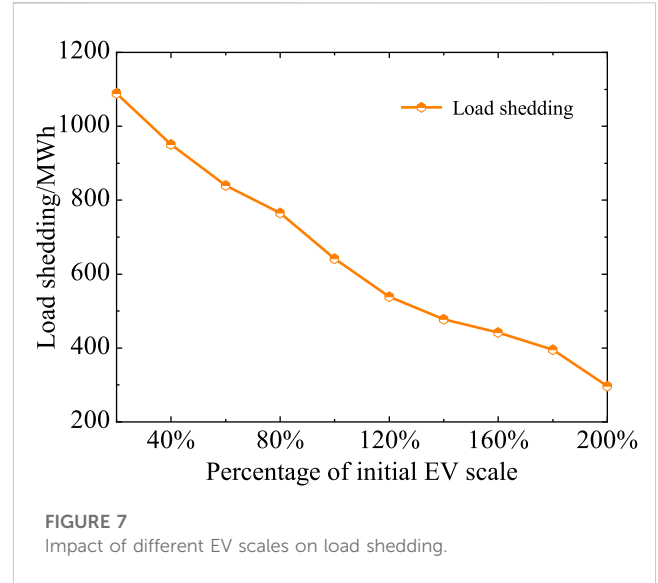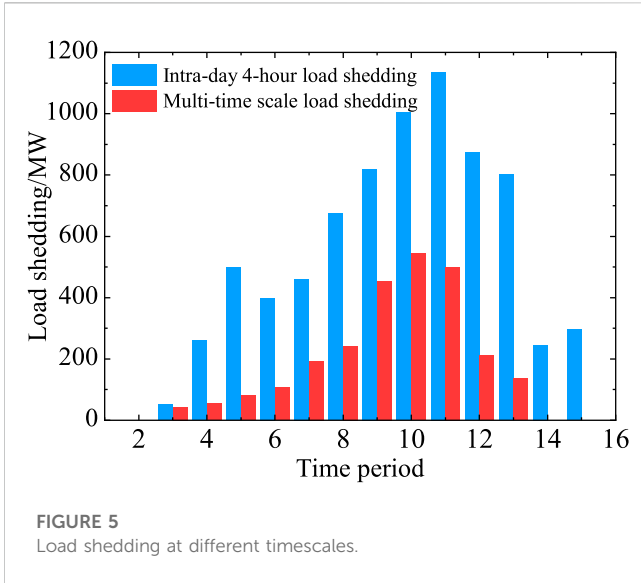
First, we analyze the impact of the integration of EV charging stations. According to Table 3, Case 2 shows a 20.49% reduction in the total system operation cost, 39.99% reduction in load shedding, and 63.87% reduction in wind spillage when compared to Case 1. Case 4 shows a 16.05% reduction in the total system operation cost, 47.21% reduction in load shedding, and 100% reduction in wind spillage when compared to Case 3. Owing to the flexibility offered by EV charging stations, the secure and

FIGURE 4
Thermal unit output adjustment at different timescales.
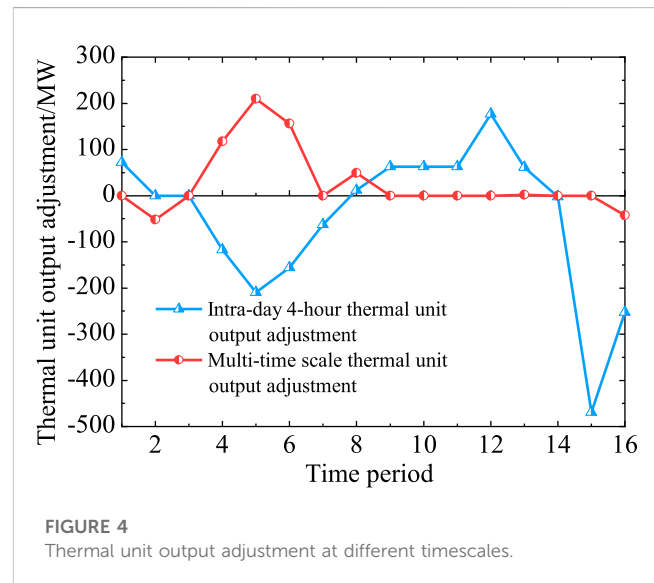
economic operation of the system is improved. Accordingly, the integration of EV charging stations can effectively address the TPB problem.

Subsequently, the impact of different timescale disposal strategies is analyzed. The results are evident by comparing the intra-day 4-h and multi-timescale disposal strategies. Without the integration of EV charging stations, Case 3 shows a 40.72% reduction in the total system operation cost, 61.21% reduction in load shedding, and 99.65% reduction in wind spillage when compared to Case 1. With the integration of EV charging stations, Case 4 exhibits a 37.41% reduction in the total system operation cost, 65.88% reduction in load shedding, and 100% reduction in wind spillage when compared to Case 2. Accordingly, the multi-timescale TPB disposal reduces the total system operation cost, load shedding, and wind spillage to varying degrees when compared to the intra-day 4-h.

The intra-day 4-h thermal unit output and multi-timescale thermal unit output adjustments are illustrated in Figure 4. According to Figure 4, the total adjustments of the intra-day 4-h and multi-timescale thermal unit outputs are 1777.86 and 628.41 MW, respectively. The total multi-timescale thermal unit output adjustment is less than that of the intra-day 4-h output. The intra-day 4-h thermal unit output adjustment significantly increases in periods 5 and 15, and the multi-timescale thermal unit output adjustment significantly increases in period 5. The situation is caused by the varying forecasting accuracies of the wind power

FIGURE 5
Load shedding at different timescales.

FIGURE 7
Impact of different EV scales on load shedding.

FIGURE 6
Impact of different EV scales on the total operation cost and thermal unit flexible ramp saving.

FIGURE 8
Three different wind power scenarios.

output and load at different timescales. In certain periods, the forecasting results of different timescales can deviate significantly, which increases the thermal unit output adjustment. The intra-day 4-h and multi-timescale load shedding for each period are depicted in Figure 5. The multi-timescale load shedding for each period is much less than that of intra-day 4-h.

The aforementioned analysis shows that the proposed multi-timescale TPB disposal can promote the disposal level of the TPB and reduce the thermal unit output adjustment more effectively than the intra-day 4-h TPB disposal strategy.

5.2 Comparison of different EV scales

To investigate the impact of different EV scales on the TPB multi-timescale disposal results, this section establishes ten scenarios

of EV scales from 20% to 200% of the initial EV scale. Under the ten scenarios, the total operation cost, thermal unit flexible ramp saving, and load shedding are illustrated in Figures 6, 7.
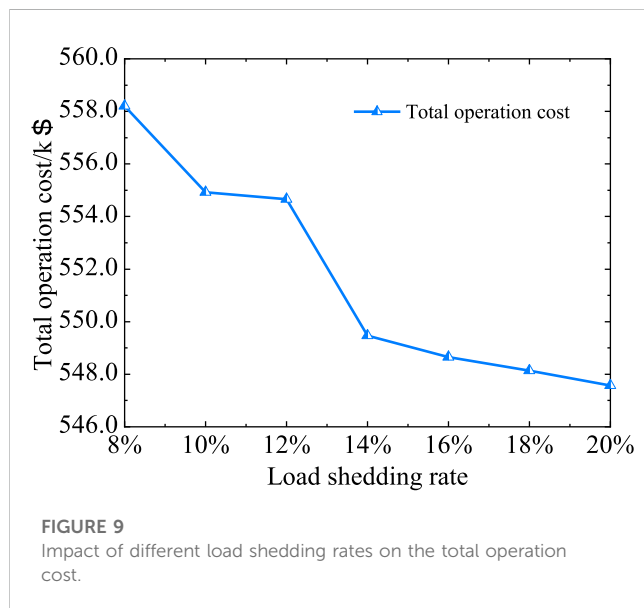
According to Figures 6, 7, as the EV scale increases, the total operation cost and load shedding decrease, and the thermal unit flexible ramp saving increases. Therefore, an increase in the EV scale promotes the disposal level of the TPB and enhances the economic operation of the system.

5.3 Comparison of different wind power scenarios

To investigate the impact of different wind power scenarios on TPB's multi-timescale disposal, three wind power scenarios are set up in this section, as shown in Figure 8.

TABLE 4 TPB multi-timescale disposal results of three wind power scenarios.

Wind power scenario	Case	Total operation cost/$	Load shedding/MWh	Wind spillage/MWh	Thermal unit flexible ramp/MWh	Thermal unit flexible ramp saving/MWh
Wind power scenario 1	Case 3	811,552.16	1,993.18	0	1,990.04	0
	Case 4	692,790.69	1,335.59	0	1,042.70	1,341.96
Wind power scenario 2	Case 3	653,011.06	1,215.44	4.35	2,083.80	0
	Case 4	548,199.35	641.66	0	1,141.53	1,356.11
Wind power scenario 3	Case 3	565,775.43	1,156.58	0	2,293.81	0
	Case 4	538,169.23	849.98	0	1,907.30	1,271.80

FIGURE 9
Impact of different load shedding rates on the total operation cost.

Wind power scenario 1: the penetration rate of wind power is 10.75%. Wind power scenario 2: the penetration rate of wind power is 21.51%. Wind power scenario 3: the penetration rate of wind power is 40.66%.

The total system operation cost, load shedding, wind spillage, thermal unit flexible ramp, and thermal unit flexible ramp savings under the three wind power scenarios are listed in Table 4.

According to Table 4, in the case of multi-timescale disposal without the integration of EV charging stations, that is, Case 3, Wind power scenario 1 exhibits the highest total operation cost and load shedding; Wind power scenario 2 has an intermediate total operation cost and load shedding; and Wind power scenario 3 has the lowest total operation cost and load shedding. In the case of multi-timescale disposal with the integration of EV charging stations, that is, Case 4, the total system operation cost, load shedding, wind spillage, thermal unit flexible ramp, and thermal unit flexible ramp savings of each wind power scenario are all decreased to a certain extent.

Therefore, the integration of EV charging stations for multi-timescale disposal can promote the disposal level of TPB under different wind power scenarios. The aforementioned analysis indicates that the proposed strategy can be applied to different

wind power scenarios, thereby verifying the effectiveness of the proposed strategy.

5.4 Comparison of different load shedding rates

To analyze the impact of different load shedding rates on the TPB multi-timescale disposal results, the total operation cost under different load shedding rates is shown in Figure 9.

According to Figure 9, as the load shedding rate increases, the total operation cost shows a decreasing trend. Therefore, the increase in load shedding rate improves the economic and security operation of the system. In addition, when the load shedding rate falls below 6% due to insufficient load shedding, the system power balance constraint cannot be met, and the proposed strategy becomes unsolvable. Therefore, to ensure the solvability of the proposed strategy, the load shedding rate should be more than 6%.

6 Conclusion

In this article, a TPB multi-timescale disposal strategy considering an EV charging station that offers flexible ramping capacity is proposed to address the TPB problem at different timescales. By analyzing the simulation results, the following conclusions can be drawn:

1) The integration of EV charging stations can offer flexible ramping capacity to the power system, thereby effectively addressing the TPB problem. The increase in the EV scale promotes the disposal level of the TPB and enhances the economic operation of the system.

2) The accuracy of wind power and load forecasting increases with a decrease in the forecasting timescale. Compared with single-timescale TPB disposal, multi-timescale TPB disposal can significantly reduce system load shedding and wind spillage.

3) Multi-timescale disposal with the integration of EV charging stations can promote the disposal level of the TPB problem under different wind power scenarios. The analysis of the simulation results indicates that the proposed strategy can be applied to different wind power scenarios, thereby verifying its effectiveness.

The focus of this article was to address the TPB issue at multi-timescales and propose a TPB multi-timescale disposal strategy for wind-integrated systems considering EV charging stations. The future research direction can include: 1) investigating the application of other flexible resources, such as dispersed energy storage and thermostatically controlled loads, to the proposed TPB multi-timescale disposal strategy and 2) extending the proposed TPB multi-timescale disposal strategy with automatic generation control (AGC) to capture 1-min timescale variability and uncertainty of wind power output.

Data availability statement

The original contributions presented in the study are included in the article/supplementary material; further inquiries can be directed to the corresponding author.

Author contributions

SY conceptualized and formed the methodology. YC prepared the original draft. JX and SY reviewed and edited the manuscript. JX supervised the study. SY administered the project. All authors have read and agreed to the published version of the manuscript.

Conflict of interest

Author SY was employed by the company China Electric Power Research Institute.

The remaining authors declare that the research was conducted in the absence of any commercial or financial relationships that could be construed as a potential conflict of interest.

Publisher's note

All claims expressed in this article are solely those of the authors and do not necessarily represent those of their affiliated organizations, or those of the publisher, editors, and reviewers. Any product that may be evaluated in this article, or claim that may be made by its manufacturer, is not guaranteed or endorsed by the publisher.

References

Bagherinezhad, A., Khatami, R., and Parvania, M. (2020). Continuous-time look-ahead flexible ramp scheduling in real-time operation. *Int. J. Electr. Power & Energy Syst.* 119, 105895. doi:10.1016/j.ijepes.2020.105895

Baniasadi, A., Habibi, D., Bass, O., and Masoum, M. (2019). Optimal real-time residential thermal energy management for peak-load shifting with experimental verification. *IEEE Trans. Smart Grid* 10 (5), 5587–5599. doi:10.1109/TSG.2018.2887232

Bessa, R., Matos, M., Soares, F., and Lopes, J. (2012). Optimized bidding of a EV aggregation agent in the electricity market. *IEEE Trans. Smart Grid* 3 (1), 443–452. doi:10.1109/TSG.2011.2159632

Chang, Y., Xie, J., Qiu, C., and Ge, Y. (2022). A disposal strategy for tight power balance considering electric vehicle charging station providing flexible ramping capacity. *IEEE Access* 10, 119805–119813. doi:10.1109/ACCESS.2022.3220671

Cui, M., and Zhang, J. (2018). Estimating ramping requirements with solar-friendly flexible ramping product in multi-timescale power system operations. *Appl. energy* 225, 27–41. doi:10.1016/j.apenergy.2018.05.031

Cui, M., Zhang, J., Wu, H., and Hodge, B. (2017). Wind-friendly flexible ramping product design in multi-timescale power system operations. *IEEE Trans. Sustain. Energy* 8 (3), 1064–1075. doi:10.1109/TSTE.2017.2647781

Ding, X., Xu, J., Sun, Y., Liao, S., and Zheng, J. (2022). A demand side controller of electrolytic aluminum industrial microgrids considering wind power fluctuations. *Prot. Control Mod. Power Syst.* 7 (4), 49–763. doi:10.1186/s41601-022-00270-x

Ghaljehei, M., and Khorsand, M. (2022). Day-ahead operational scheduling with enhanced flexible ramping product: Design and analysis. *IEEE Trans. Power Syst.* 37 (3), 1842–1856. doi:10.1109/TPWRS.2021.3110712

Han, H., Wei, T., Wu, C., Zang, H., Sun, G., Wei, Z., et al. (2022). A low-carbon dispatch strategy for power systems considering flexible demand response and energy storage. *Front. Energy Res.* 10. doi:10.3389/fenrg.2022.883602

Heydarian-Forushani, E., Golshan, M., and Shafie-Khah, M. (2015). Flexible security-constrained scheduling of wind power enabling time of use pricing scheme. *Energy* 90, 1887–1900. doi:10.1016/j.energy.2015.07.014

Heydarian-Forushani, E., Golshan, M., Shafie-khah, M., and Siano, P. (2018). Optimal operation of emerging flexible resources considering sub-hourly flexible ramp product. *IEEE Trans. Sustain. Energy* 9 (2), 916–929. doi:10.1109/TSTE.2017.2766088

Hu, C., Cai, Z., Zhang, Y., Yan, R., Cai, Y., and Cen, B. (2022). A soft actor-critic deep reinforcement learning method for multi-timescale coordinated operation of microgrids. *Prot. Control Mod. Power Syst.* 7 (3), 29–432. doi:10.1186/s41601-022-00252-z

Khoshjahan, M., Dehghanian, P., Moeini-Aghtaie, M., and Fotuhi-Firuzabad, M. (2019). Harnessing ramp capability of spinning reserve services for enhanced power grid flexibility. *IEEE Trans. Industry Appl.* 55 (6), 7103–7112. doi:10.1109/TIA.2019.2921946

Khoshjahan, M., Moeini-Aghtaie, M., Fotuhi-Firuzabad, M., Dehghanian, P., and Mazaheri, H. (2020). Advanced bidding strategy for participation of energy storage systems in joint energy and flexible ramping product market. *IET Generation, Transm. Distribution* 14 (22), 5202–5210. doi:10.1049/iet-gtd.2020.0224

Li, W., Liang, R., Luo, F., Feng, S., Yang, B., Liu, Z., et al. (2022). Response potential assessment of user-side flexible resources of regional power distribution networks based on sequential simulation of optimal operation. *Front. Energy Res.* 10. doi:10.3389/fenrg.2022.1096046

Mirzaei, M. A., Sadeghi-Yazdankhah, A., Mohammadi-Ivatloo, B., Marzband, M., Shafie-khah, M., and Catalão, J. P. (2019). Integration of emerging resources in IGDT-based robust scheduling of combined power and natural gas systems considering flexible ramping products. *Energy* 189, 1–116195. doi:10.1016/j.energy.2019.116195

Mueller, F., Woerner, S., and Lygeros, J. (2019). Unlocking the potential of flexible energy resources to help balance the power grid. *IEEE Trans. Smart Grid* 10 (5), 5212–5222. doi:10.1109/TSG.2018.2878998

Neyestani, N., Damavandi, M., Shafie-Khah, M., Contreras, J., and Catalão, J. (2015). Allocation of plug-in vehicles' parking lots in distribution systems considering network-constrained objectives. *IEEE Trans. Power Syst.* 30 (5), 2643–2656. doi:10.1109/TPWRS.2014.2359919

Nikoobakht, A., Aghaei, J., Shafie-Khah, M., and Catalao, J. P. (2019). Assessing increased flexibility of energy storage and demand response to accommodate a high penetration of renewable energy sources. *IEEE Trans. Sustain. Energy* 10 (2), 659–669. doi:10.1109/TSTE.2018.2843161

Olsen, K., Zong, Y., You, S., Bindner, H., Koivisto, M., and Gea-Bermúdez, J. (2020). Multi-timescale data-driven method identifying flexibility requirements for scenarios with high penetration of renewables. *Appl. Energy* 264, 114702. doi:10.1016/j.apenergy.2020.114702

Park, H., Huang, B., and Baldick, R. (2022). Enhanced flexible ramping product formulation for alleviating capacity shortage in look-ahead commitment. *J. Mod. Power Syst. Clean Energy* 10 (4), 850–860. doi:10.35833/MPCE.2020.000942

Shaaban, M., Tan, W., and Abdullah, M. (2018). A multi-timescale hybrid stochastic/deterministic generation scheduling framework with flexiramp and cycliramp costs. *Int. J. Electr. Power & Energy Syst.* 99, 585–593. doi:10.1016/j.ijepes.2018.02.004

Shafie-Khah, M., Heydarian-Forushani, E., Osório, G., Gil, F., Aghaei, J., Barani, M., et al. (2016). Optimal behavior of electric vehicle parking lots as demand response aggregation agents. *IEEE Trans. Smart Grid* 7 (6), 2654–2665. doi:10.1109/TSG.2015.2496796

Su, W., and Chow, M. (2012). Computational intelligence-based energy management for a large-scale PHEV/PEV enabled municipal parking deck. *Appl. Energy* 96, 171–182. doi:10.1016/j.apenergy.2011.11.088

Wang, Q., and Hodge, B. (2017). Enhancing power system operational flexibility with flexible ramping products: A review. *IEEE Trans. Industrial Inf.* 13 (4), 1652–1664. doi:10.1109/TII.2016.2637879

Wu, H., Shahidehpour, M., Alabdulwahab, A., and Abusorrah, A. (2015). Thermal generation flexibility with ramping costs and hourly demand response in stochastic security-constrained scheduling of variable energy sources. *IEEE Trans. Power Syst.* 30 (6), 2955–2964. doi:10.1109/TPWRS.2014.2369473

Yamujala, S., Jain, A., Sreekumar, S., Bhakar, R., and Mathur, J. (2022). Enhancing power systems operational flexibility with ramp products from flexible resources. *Electr. Power Syst. Res.* 202, 107599. doi:10.1016/j.epsr.2021.107599

Zhang, B., and Kezunovic, M. (2016). Impact on power system flexibility by electric vehicle participation in ramp market. *IEEE Trans. Smart Grid* 7 (3), 1285–1294. doi:10.1109/TSG.2015.2437911

Zhang, X., Che, L., Shahidehpour, M., Alabdulwahab, A., and Abusorrah, A. (2016). Electricity-natural gas operation planning with hourly demand response for deployment of flexible ramp. *IEEE Trans. Sustain. Energy* 7 (3), 996–1004. doi:10.1109/TSTE.2015.2511140

Zhang, X., Hu, J., Wang, H., Wang, G., Chan, K. W., and Qiu, J. (2020). Electric vehicle participated electricity market model considering flexible ramping product provisions. *IEEE Trans. Industry Appl.* 56 (5), 5868–5879. doi:10.1109/TIA.2020.2995560